8030 J. Med. Chem. 2010, 53, 8030–8040
DOI: 10.1021/jm100771s

Journal of Medicinal Chemistry Article

Effects on Molecular Conformation and Anticoagulant Activities of 1,6-Anhydrosugars at the Reducing Terminal of Antithrombin-Binding Octasaccharides Isolated from Low-Molecular-Weight Heparin Enoxaparin

Marco Guerrini,[†] Stefano Elli,[†] Davide Gaudesi,[†] Giangiacomo Torri,[†] Benito Casu,[†] Pierre Mourier,[‡] Frederic Herman,[‡] Christian Boudier,[§] Martin Lorenz,[‡] and Christian Viskov*[,‡]

[†]"G. Ronzoni" Institute for Chemical and Biochemical Research, via G. Colombo 81, 20133 Milan, Italy, [‡]Sanofi-Aventis, 13 Quai Jules Guesde, 94403 Vitry sur Seine, France, and [§]CNRS UMR 7175, Département Physicochimie et Pharmacochimie des Interactions Moléculaires et Cellulaires, Faculté de Pharmacie, Université Louis Pasteur, Strasbourg I, F 67401, France

Received June 23, 2010

Terminal 1,6-anhydro-aminosugars (1,6-anAS) are typical structural moieties of enoxaparin, a low-molecular-weight heparin (LMWH) widely used for prevention and treatment of thrombotic disorders. In the enoxaparin manufacturing process, these modified amino sugars are formed during the β-eliminative cleavage of heparin. To investigate the effect of terminal anAS on antithrombin (AT) binding and on inhibition of factor Xa (FXa), two octasaccharides containing modified AT-binding pentasaccharide sequences were isolated from enoxaparin. The molecular conformation of the octasaccharides terminating with *N*-sulfo-1,6-anhydro-D-mannosamine and *N*-sulfo-1,6-anhydro-D-glucosamine, respectively, has been determined both in the absence and presence of AT by NMR experiments and docking simulations. Reduced overall contacts of the terminal anAS residues with the binding region of AT induce a decrease in affinity for AT as well as lower anti-FXa activity. The anti-FXa measured either in buffer or plasma milieu does not show any significant difference, suggesting that the inhibition of anti-FXa remains specific and biologically relevant.

Introduction

Low-molecular-weight heparins (LMWHs[a]), which are obtained from heparin by enzymatic or chemical depolymerization, are widely used in clinics for prevention and treatment of thromboembolism.[1,2] The lower molecular size of LMWHs, compared with heparin, involves a more predictable pharmacological action, sustained antithrombotic activity, and better subcutaneous bioavailability.[3] Like heparin, LMWHs are constituted by repeating disaccharide units of uronic acid (β-D-glucuronic, G, or α-L-iduronic, I) and α-D-glucosamine (GlcN) residues, with varying patterns of sulfation, at position-2 of the uronic acid, at position-6, and more rarely at position-3 of the glucosamine residues, which are mainly *N*-sulfated and occasionally *N*-acetylated.[4]

Heparin elicits its anticoagulant and antithrombotic activity through binding to several plasma proteins. Especially relevant for the antithrombotic properties, heparin enhances ~1000-fold the activity of the endogenous coagulation inhibitor antithrombin (AT) to inhibit the key coagulation proteases: thrombin and factor Xa (FXa). Heparin binds to AT via the pentasaccharide sequence GlcNAc,6SO_3−GlcA−GlcNSO_3,3,6SO_3*−IdoA2SO_3−GlcNSO_3,6SO_3 (commonly abbreviated A_{NA}GA*I_SA). Natural variant compatible with high affinity for AT having *N*-sulfation instead of *N*-acetylation of the first aminosugar residue is also present, especially in bovine heparin.[5] LMWHs consist of complex mixture of fragments ranging from tetra to hexadecasaccharides and somewhat higher oligosaccharides.[6−8] Apart from tetrasaccharides, about one out of five chains of LMWHs contain the active sequence A_{NA}GA*I_SA.[7] This proportion of the AT binding oligosaccharides is not constant in LMWH fractions. In enoxaparin, it increases from 3% to 5% in the hexasaccharide fraction to 20% in hexadecasaccharides.[6] The smallest A_{NA}GA*I_SA containing fragments inactivate FXa as efficiently as longer heparin chains but have a reduced ability to inactivate thrombin because their molecules cannot bridge over thrombin and AT to form the necessary ternary complex.[9,10] However, only a small amount of fragments of above hexadecasaccharides, contained in enoxaparin, exhibits significant antithombin activity (anti FIIa), explaining its greater inhibitory activity against FXa than against FIIa (anti-FXa/anti-FIIa activity ratio ~3.8).[6] Extensive studies on natural and synthetic oligosaccharides permitted identification of the functional groups of A_{NA}GA*I_SA essential for high-affinity

*To whom correspondence should be addressed. Phone: +33-158-938638. Fax: +33-158-933908. E-mail: Christian.Viskov@sanofi-aventis.com.

[a] Abbreviations: 1,6-anAS, 1,6-anhydro-aminosugars; LMWH, low-molecular weight heparin; AT, antithrombin; FXa, factor Xa; G, GlcA (β-D-glucuronic acid acid); I, IdoA (α-L-iduronic acid); GlcN, α-D-glucosamine; A_{NA}, GlcNAc,6SO_3 (*N*-acetylated-6-*O*-sulfated-D-glucosamine); A*, GlcNSO_3,3,6SO_3 (*N*-sulfated-3,6-*O*-sulfated-D-glucosamine); A, GlcNSO_3,6SO_3 (*N*-sulfated-6-*O*-sulfated-D-glucosamine); I_S, IdoA2SO_3 (2-*O*-sulfated-L-iduronic acid); 1,6-anG, *N*-sulfo-amino-1,6-anhydro-2-deoxy-β-D-glucopyranose; 1,6-anM, *N*-sulfo-amino-1,6-anhydro-2-deoxy-β-D-mannopyranose; STD, saturation-transfer-difference; trNOESY, transferred nuclear Overhauser effect spectroscopy; CTA-SAX, cetyl trimethyl ammonium strong anion-exchange; GPC, gel permeation chromatographic; COSY, homonuclear correlation spectroscopy; TOCSY, total correlation spectroscopy; HSQC, heteronuclear-single-quantum-coherence; ΔU_S, 2-*O*-sulfated 4,5-unsaturated uronic acid; $^3J_{H-H}$, three bonds proton−proton coupling constants; ROESY, rotating frame Overhauser effect spectroscopy;

 Published on Web 10/28/2010

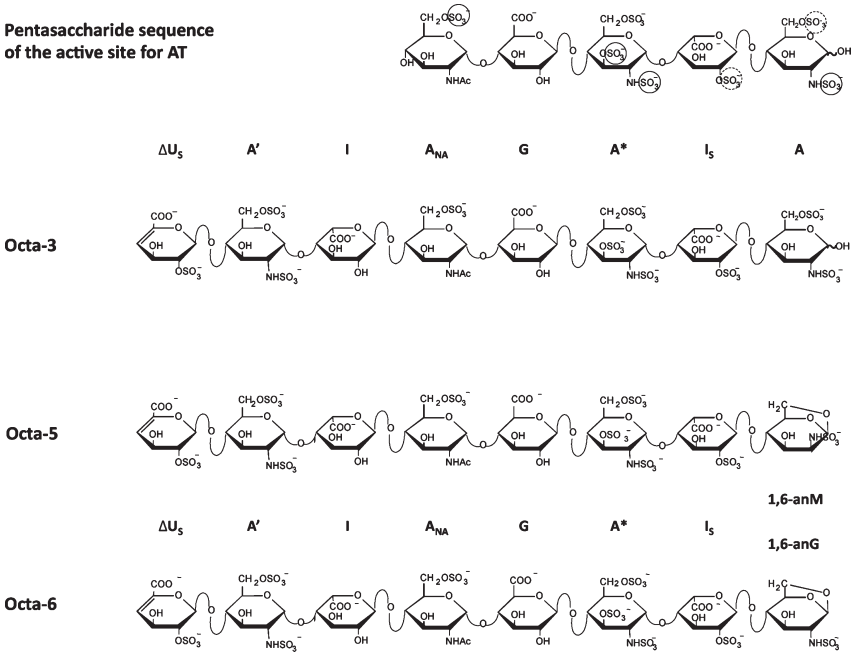

Figure 1. Structure of octasaccharides Octa-5 and Octa-6 in comparison with that of the pentasaccharide sequence of the active site for AT and Octa-3. Groups highlighted in the circles are essential groups for the activation of AT, and those highlighted by dashed circles are also important but not essential contributors to affinity for AT.

binding to AT.[4,10] These functional groups (circled in the formula of $A_{NA}GA^*I_SA$ in Figure 1) are the 6-*O*-sulfate of the first *N*-acetylated-6-*O*-sulfated-glucosamine (A_{NA}) residue, the *N*- and 3-*O*-sulfates of the *N*-sulfated-3,6-*O*-sulfated-glucosamine (A*), and the *N*-sulfate of the terminal *N*-sulfated-6-*O*-sulfated-glucosamine (A) at the "reducing" end of $A_{NA}GA^*I_SA$. In addition, the unmodified glucuronic acid residue was demonstrated to be essential for high-affinity binding to AT.[4,10] The 2-*O*-sulfate group of the 2-*O*-sulfated iduronic acid residue (I_S) was shown to contribute to the binding to AT only indirectly by favoring the $^2S_0$ conformation of the iduronate ring. Indeed, the 2-OSO_3 group appears to be the main driving force in affecting the shift of the conformational equilibrium of the sulfated iduronate residue toward the skewboat form, thus enhancing dipolar contact between the AGA*IA reducing disaccharides with AT amino acids.[11] However, the contribution of the I_S to the AT affinity may be less essential when the size of oligosaccharides is larger than octasaccharide.[12] The question whether the 6-*O*-sulfate group of the A residue at the reducing end of $A_{NA}GA^*I_SA$ contributes to binding to AT remains open. Whereas its absence in synthetic pentasaccharides results in a decrease in the affinity for AT,[13] NMR and molecular modeling studies on Octa-3 indicated that this group has no interacting contacts with the AT.[14] However, the presence of 6-*O*-sulfate group increases the population of $^2S_0$ form of the neighbor I_S residue,[15] contributing to a better docking of the pentasaccharide to AT.

Although the depolymerization method of heparin used to generate LMWHs affects the structure of the resulting fragments,[6] LMWHs obtained with different depolymerization methods differ from each other in the type of reducing and nonreducing residues at the cleavage sites of the heparin chains.[16,17] Among LMWHs, enoxaparin, obtained by alkaline hydrolysis of benzyl esters of heparin, has a particular complex structural profile, as indicated by the presence of modified terminal residues. Some of them are unique and represent characteristic fingerprints of the enoxaparin mixture of heparin fragments when compared to other LMWHs.[16,17] In particular, the presence at the reducing end of two unique bicyclic structures originated from alkaline treatment of the benzyl esters of heparin is a major distinctive characteristics of enoxaparin, raising the question whether they contribute to the affinity for AT and the anti-Xa activity of this LMWH. The structure of these residues have been defined as *N*-sulfo-amino-1,6-anhydro-2-deoxy-β-D-glucopyranose (1,6-anG) and *N*-sulfo-amino-1,6-anhydro-2-deoxy-β-D-mannopyranose (1,6-anM).[18]

Terminal 1,6-anG and 1,6-anAM were identified also in enoxaparin fractions with high affinity for AT.[7] However, whether these residues constituted a modification of the terminal A residue of $A_{NA}GA^*I_SA$, or the active sequence was further inside the oligosaccharide chain, cannot be determined without isolation and structural characterization of individual components with high affinity for AT. The active role of residues prolonging the pentasaccharide sequence toward both its reducing and nonreducing end was recently demonstrated for some octasaccharides isolated from enoxaparin.[14,19] The affinity of these octasaccharides for AT depends not only on the location of the pentasaccharidic sequence $A_{NA}GA^*I_SA$ along the oligosaccharide chain but may be also strongly affected by the structure that prolong that sequence. Notably, the presence of glucuronic acid instead of iduronic acid before the pentasaccharide moiety increases one order of magnitude the affinity toward AT.[19] Because the total octasaccharide fraction represents a significant component of enoxaparin (about the 15% (w/w)),[7] individual octasaccharides containing intact or partially modified $A_{NA}GA^*I_SA$ sequences are useful models to study the effects of octasaccharides structural variations on AT binding.

In the present work, two novel octasaccharides incorporating the active pentasaccharide sequence with a modified aminosugar at the reducing end were isolated from enoxaparin. In these octasaccharides, the most common *N*-sulfo-6-*O*-sulfated-glucosamine residue (A) at the reducing end of the

$A_{NA}GA^*I_SA$ sequence (Octa-3 of a previous study)[19] is substituted by a 1,6-anM (Octa-5) and 1,6-anG (Octa-6) residues (Figure 1). Although these two octasaccharides showed significantly lower affinity to AT as well as a reduced anti-FXa activity when compared with the pentasaccharide fondaparinux (the α-methyl glycoside of a synthetic version of $A_{NA}GA^*I_SA$ with *N*-SO_3 instead of *N*-acetyl group at the nonreducing aminosugar residue) and with the $A_{NA}GA^*I_SA$ containing octasaccharides so far described, they display essentially the same anti-FXa activity in plasma and in buffer solution, which supports the concept that they specifically interact with AT.

The structure and conformational properties of complexes of Octa-5 and Octa-6 with AT were investigated in solution by saturation transfer difference (STD), transferred-nuclear-Overhauser-effect-spectroscopy (trNOESY) NMR experiments, while docking simulations were used to build complex geometries agreeing to the experimental data. Our results confirm that the unmodified *N*-sulfo-6-*O*-sulfated-glucosamine residue at the reducing end is important for an efficient binding to AT and indicate that the terminal 1,6anAS of Octa-5 and Octa-6 are not completely involved in the binding, thus explaining the lower affinity to AT and a reduced anti-FXa activity of these octasaccharides compared to the octasaccharide Octa-3, terminating with unmodified A residue. Results of this study also explain the somewhat higher affinity for AT (and also activity) of the *manno* vs *gluco* isomer of 1,6-anhydro variants of the octasaccharides.

Results

Isolation and Characterization of Octasaccharides. Isolation of the octasaccharide Octa-3 was previously described.[19] Octasaccharides Octa-5 and Octa-6 were obtained by combining AT affinity chromatography, strong anion-exchange on Carbopack AS11-HC (Dionex), and cetyl trimethyl ammonium strong anion-exchange (CTA-SAX) chromatography on a semipreparative scale, starting from an octasaccharide gel permeation chromatographic (GPC) fraction of enoxaparin. GPC of enoxaparin and the desalting conditions of the selected fractions were performed as described previously.[20]

The octasaccharide fraction was chromatographed on an AT Sepharose column (40 cm × 5 cm) with a stepwise gradient of NaCl. The column was prepared by coupling human AT (1 g) to CNBr-activated Sepharose 4B (Sigma) according to Höök et al.[21] In a first separation, octasaccharides from enoxaparin were injected on the affinity column under slightly overloading conditions (750 mg injected at each run). The low- and medium-affinity portions were eluted from the column with a 0.25 M NaCl solution buffered at pH 7.4 with 1 mM Tris-HCl at 6 mL/min. The high-affinity octasaccharide fractions were eluted with a step gradient of NaCl (range between 0.25 and 3 M NaCl, 1 mM Tris-HCl, pH 7.4). The NaCl gradient was monitored by conductivity measurements, and the octasaccharides in the effluents were detected by UV at 232 nm. Octasaccharides eluted in low-affinity fractions were collected and desalted on Sephadex G-10 and reinjected (200 mg at each run) on the affinity column using the same step gradient of NaCl. Octasaccharides were mainly eluted in the low affinity fraction, with a small part eluted in affine fractions at conductivities between 25 and 80 mS/cm. Octa-5 and Octa-6 were mainly eluted in the affine fraction but in part also in the tail of the low-affinity peak. Fractions were controlled using analytical Carbopack AS11 column (Dionex 250 mm × 2.1 mm) circulated with $NaClO_4$ solution at concentration varying between 0 and 0.6N and buffered at pH 3 using 2.5 mM NaH_2PO_4. Fractions containing Octa-5 and Octa-6 were collected and desalted as previously. The final purification was achieved in three steps: a first purification was done on Carbopack AS11-HC (Dionex) semipreparative columns (250 cm × 20 cm). The mobile phase was a $NaClO_4$, pH 3, aqueous solution at concentrations varying between 0 and 0.6 N circulated in the column at 20 mL/min. Fractions were controlled using analytical CTA-SAX chromatography. Purified octasaccharides were then desalted on Sephadex G10 and injected on a CTA-SAX semipreparative column (25 cm × 2.2 cm) prepared as described previously[20] and filled with Hypersil BDS C18 (5 μm particle size). Mobile phases for oligosaccharide separation were aqueous sodium methane sulfonate pH 3 (Interchim) at concentrations varying between 0 and 2.5 M. Separations were achieved at 40 °C. Salt concentration in the mobile phase was increased linearly from 0 to 2.5 M over 60 min. Flow rate was 20 mL/min and UV detection at 234 nm was used. Collected fractions were neutralized and desalted on Sephadex G-10 after a preliminary treatment on Mega Bondelut C18 cartridges (Varian). Analytical control of the fractions was done in CTA-SAX as previously. In this separation, Octa-5 and Octa-6 could be almost totally resolved. A last purification was done on Carbopack AS11-HC semipreparative columns using the same conditions as in the first separation step. Purified Octa-5 and Octa-6 were then desalted on Sephadex G10 and lyophilized. Octa-5 and Octa-6 were assayed by CTA-SAX HPLC chromatography, and their purity in 1,6 anhydro derivatives was 89% and 84%, respectively (Supporting Information Figure S2). Because of complex separation of Octa-5 and Octa-6, each of them contains minor amounts of each other (18% and 10%, respectively); this is pointed out by the anomeric signal integrations of the proton spectra (Figure 2).

Equilibrium Dissociation Constants for the Octasaccharide−AT complexes. Saturation of constant amounts of AT by increasing quantities of Octa-3, -5, and -6 resulted in a ±30% increase of the protein intrinsic fluorescence as observed for the pentasaccharide AGA^*I_SA (fondaparinux), the reference product. Fluorescence data were satisfactorily analyzed by assuming a 1:1 binding stoichiometry as already reported[19] to determine the best estimates of K_d the equilibrium dissociation constant. Its values for the various oligosaccharides: AT pairs are listed in Table 1. We found that in 0.05 M HEPES, 0.1 M NaCl K_d for Octa-5-AT and Octa-6-AT complexes is equal to 0.90 ± 0.08 and 1.23 ± 0.06 μM, an affinity about 50- and 10-fold lower than that determined for the fondaparinux and Octa-3 under the same conditions: 0.021 ± 0.001 and 0.12 μM, respectively. Because of their moderate affinity, it was not possible to determine K_d for the binding of Octa-5 and -6 to AT in the presence of higher salt concentration.

Anti-FXa Activity of Octasaccharides. The anti-FXa activity using a purified factor Xa and AT was measured in buffer as well as in human plasma for both octasaccharides. Enoxaparin and the synthetic pentasaccharide fondaparinux were tested as reference agents (Table 2). A specific activity of 120 anti-FXa units/mg in buffer was measured for enoxaparin, which is in the known specification range.[22] The activity of fondaparinux of 810 anti-FXa units/mg is in line with historical data.[23]

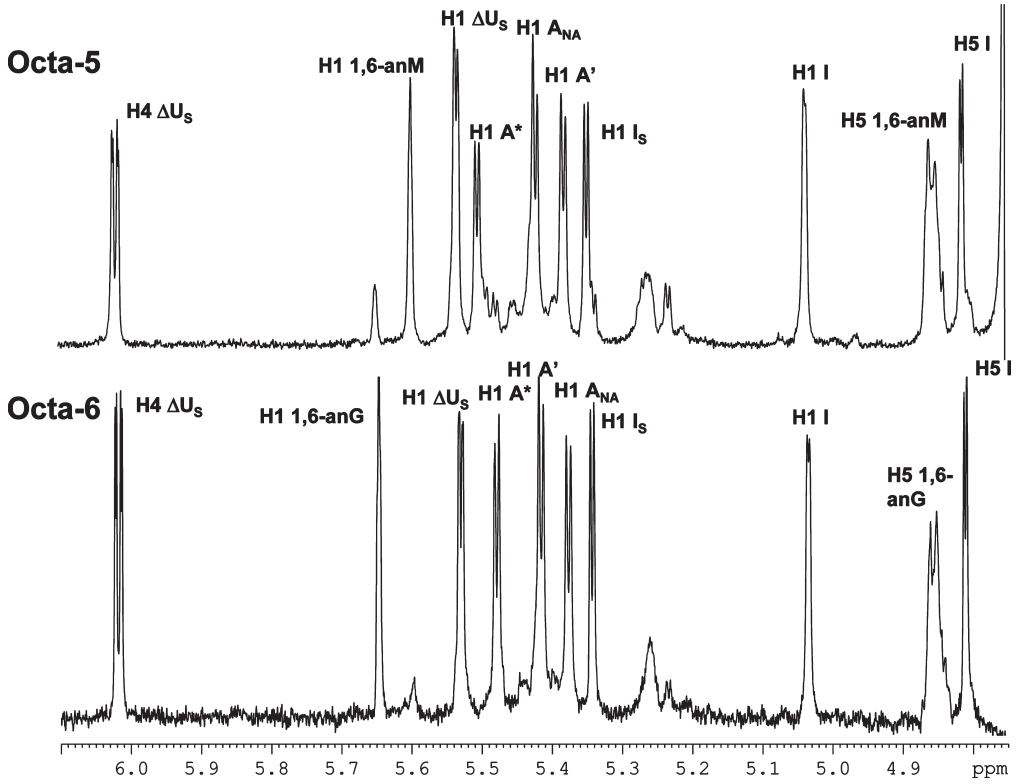

Figure 2. Partial 900 MHz ^{1}H NMR spectra of Octa-5 and Octa-6.

Table 1. Equilibrium Dissociation Constant K_d (μM) for the Interaction of Human AT with Octa-5, Octa-6, and Octa-3 Oligosaccharides Purified from enoxaparin with Respect That of the Pentasaccharide fondaparinux Determined at 25 °C in 0.05 M HEPES, pH 7.4 Containing 0.1, 0.25, or 0.5 M NaCl

[NaCl] (M)	Octa-5	Octa-6	Octa-3	fondaparinux
0.10	0.90	1.23	0.12	0.0207
0.25	> 10 μM	> 10 μM	nd	0.279
0.50	nd	nd	2.74	3.46

Table 2. Specific Anti-FXa Activity Measured in Human Plasma and Aqueous Buffer Solution[a]

	anti-FXa activity (U/mg)	
compd	buffer	plasma
enoxaparin	120.0 ± 0.9	104.2 ± 1.3
fondaparinux	810.1 ± 10.8	761 ± 11.3
Octa-5	51.4 ± 0.8	49.6 ± 0.4
Octa-6	39.6 ± 0.9	39.3 ± 0.8

[a] Data represent mean ± SEM $n = 5$. Assay calibration was performed against the Second International Standard for LMWH, code no. 01/608.

The anti-FXa activity in human plasma for enoxaparin and fondaparinux was slightly lower (13% and 6%) compared to that in an aqueous buffer solution. In contrast, Octa-5 and Octa-6 showed a lower anti-FXa activity of approximately 50 and 40 anti-FXa units/mg, respectively, but no difference in their anti-FXa-activity in plasma and in aqueous buffer solution.

NMR Characterization of Octasaccharides 5 and 6. The anomeric regions of proton spectra of Octa-5 and Octa-6 are shown in Figure 2. Proton and carbon resonances (Tables 3 and 4) were assigned using standard homonuclear correlation spectroscopy (COSY) and total-correlation spectroscopy (TOCSY) (not shown) and heteronuclear-single-quantum-coherence (HSQC) spectroscopy (Supporting Information Figures S3−S4). NOESY experiments were performed to sequentially connect saccharide ring systems (Supporting Information Figures S5−S6). The two octasaccharides, differing in the C-2 epimerization of their 1,6-anydro-hexosamine residues, show significant ^{1}H and ^{13}C chemical shift differences of 1,6-anAS resonances and of the preceding I_S residues (Tables 3 and 4). Small differences of proton and carbon chemical shifts found for reducing 1,6-anAS residues with respect to those previously observed for disaccharides can be ascribed to the different types of uronic acid to which they are linked. In fact, the largest differences have been observed for the H4/C4 atoms, which are involved in the linkage with the I_S residue in octasaccharides and with the 2-*O*-sulfated 4,5-unsaturated uronic acid (ΔU_S) residues in disaccharides (Tables 3 and Supporting Information Tables S11−S12).[24] The three bonds proton−proton coupling constants ($^3J_{H-H}$) of the 1,6-anAS residues, measured on octasaccharides (Table 3), disaccharide, and tetrasaccharide models (Supporting Information Tables S11−S12), indicate that both of these residues assume the $^1C_4$ conformation.[24,25] Moreover, the ROESY spectrum indicates a dipolar interaction between H-4 and H-6a of 1,6-anAS residues, which implies that the 1,6-cycle is located above the pyranose ring (Supporting Information Figure S7). The conformation of uronate residues within and preceding the AGA*IA sequence were analyzed by $^3J_{H-H}$ and NOEs (Tables 3, 6 and 7). The measured values of $^3J_{H1-H2}$ and of $^3J_{H4-H5}$ of unsaturated uronic acid moiety of both octasaccharides indicated a preferred $^1H_2$ half-chair conformation of such residue, as observed for similar octasaccharides.[14] In both octasaccharides, the measured values of $^3J_{H1-H2}$ and of $^3J_{H4-H5}$ of sulfated iduronic acid moiety within AGA*IA sequence (I_S) are

Table 3. 600 MHz Proton Chemical Shifts (in ppm) and $^3J_{HH}$ Coupling Constants (in Hz) of Octasaccharide-**5** (a) and Octasaccharide-**6** (b) Residues Measured at 30 °C in Phosphate Buffer 10 mM, pH 7.4, and 0.15 M NaCl[a]

(a)

	ΔU_S	A′	I	A_{NA}	G	A*	I_S	1,6-anM
H1	5.533	5.379	5.038	5.418	4.639	5.503	5.344	5.598
$^3J_{H1-H2}$	*3.1*	*3.9*	*2.3*	*3.8*	*8.2*	*3.5*	*3.3*	*1.9* (*1.8*)
H2	4.653	3.311	3.813	3.962	3.414	3.491	4.377	3.503
$^3J_{H2-H3}$								*5.2* (*5.4*)
H3	4.353	3.674	4.157	3.798	3.732	4.411	4.237	4.085
$^3J_{H3-H4}$							*3.6*	(*< 2*)
H4	6.018	3.866	4.101	3.758	3.82	4.002	4.183	4.011
$^3J_{H4-H5}$	*4.7*		*2.4*				*3.0*	(*1.6*)
H5		4.008	4.811	4.052	3.82	4.169	4.608	4.854
$^3J_{H5-H6a}$								(*0.9*)
$^3J_{H5-H6b}$								(*5.9*)
H6a		4.393		4.367		4.541		4.299
$^3J_{H6a-H6b}$								(*7.8*)
H6b		4.245		4.241		4.284		3.797

(b)

	ΔU_S	A′	I	A_{NA}	G	A*	I_S	1,6-anG
H1	5.544	5.390	5.046	5.428	4.652	5.491	5.355	5.661
$^3J_{H1-H2}$	*3.0*	*3.8*	*2.1*	*3.9*		*3.5*	*3.1*	(*< 2*)
H2	4.666	3.320	3.826	3.970	3.424	3.504	4.407	3.255
$^3J_{H2-H3}$								(*< 2*)
H3	4.364	3.686	4.163	3.822	3.744	4.432	4.267	3.948
$^3J_{H3-H4}$								(*< 2*)
H4	6.029	3.875	4.112	3.766	3.821	4.003	4.198	3.869
$^3J_{H4-H5}$	*4.7*		*2.4*				*2.9*	(*< 2*)
H5		4.010	4.823	4.061	3.821	4.541	4.696	4.868
$^3J_{H5-H6a}$								(*1.2*)
$^3J_{H5-H6b}$								(*5.8*)
H6a		4.402		4.375		4.525		4.261
$^3J_{H6a-H6b}$								(*7.8*)
H6b		4.253		4.253		4.303		3.82

[a] $^3J_{H1-H2}$ couplings in parentheses were measured on tetra- and disaccharide models having 1.6 anM and 1.6 anG residue at the reducing end, respectively (Supporting Information Figures S7−S9, Tables S11−S12).

Table 4. 600 MHz Carbon Chemical Shifts (in ppm) of Octa-**5** (a) and Octa-**6** (b) Measured at 30 °C in Phosphate Buffer 10 mM, pH 7.4 and 0.15 M NaCl

(a)

	ΔU_S	A′	I	A_{NA}	G	A*	I_S	1,6-anM
C1	100.22	98.48	104.83	99.83	103.86	99.15	102.39	103.76
C2	77.41	60.03	71.40	56.64	76.39	59.45	79.68	55.03
C3	65.67	72.48	70.50	71.40	79.18	79.12	72.57	71.16
C4	108.91	80.97	77.57	80.18	80.1	75.82	78.75	80.83
C5		71.32	71.92	80.1	72.45	72.34	76.48	76.58
C6		69.03		69.03		68.79		67.83

(b)

	ΔU_S	A′	I	A_{NA}	G	A*	I_S	1,6-anG
C1	100.02	98.48	104.83	99.83	103.86	99.29	100.91	104.13
C2	77.41	60.23	71.40	56.64	76.39	59.45	79.12	58.48
C3	65.67	72.48	70.50	71.40	79.18	79.12	72.08	73.02
C4	108.98	80.97	77.67	80.18	80.1	75.82	78.65	79.03
C5		71.58	71.32	72.02	80.1	72.45	72.13	76.24
C6		69.03		69.03		68.79		67.73

compatible with the presence of both $^1C_4$ and $^2S_0$ forms contributing to the conformational equilibrium of these moieties, similarly to what was observed in I_S residues of all previously described octasaccharides.[14,19] However, the $^3J_{H1-H2}$ and $^3J_{H4-H5}$ values of I_S measured on Octa-5 ($^3J_{H1-H2}$ 3.3 Hz and $^3J_{H4-H5}$ 3.0 Hz) and Octa-6 ($^3J_{H1-H2}$ 3.1 Hz and $^3J_{H4-H5}$ 2.9 Hz) spectra are smaller than those measured on Octa-3 ($^3J_{H1-H2}$ 3.8 Hz and $^3J_{H4-H5}$ 3.1 Hz),[14] accounting for larger contribution of the $^2S_0$ form to the I_S conformational equilibrium of the latter octasaccharide. This difference suggests that the steric hindrance generated by the reducing bicyclic anhydro ring disfavors the $^2S_0$ form (Supporting Information Table S11).

In contrast, the nonsulfated iduronic acid residues (I) preceding the $A_{NA}GA^*I_SA$ sequence shows smaller $^3J_{H1-H2}$ and $^3J_{H4-H5}$ values (Table 3), compatible with a minor contribution of the $^2S_0$ form. Because the $^1C_4$ and $^2S_0$ conformations exhibit distinct H5−H2 distances, the observed NOE value can be considered as marker of the presence of $^2S_0$ conformation.[15,26] In both octasaccharide 5 and 6, I and I_S show detectable H5−H2 NOE, which confirms a contribution of the $^2S_0$ form to the conformational equilibrium of these residues (Table 6−7). No significant difference of the conformational equilibrium of I and I_S between the two octasaccharides was observed.

STD Experiments. Protocol based on STD NMR spectra is one of the most useful methods to characterize the binding interactions at the atomic level of a ligand to a protein target. The experimental protocol is based on the transfer of saturation from the protein to bound ligands that, exchanging into solution between free and bound state, allows utilizing the free ligand signals for detection. The building block of the ligand having the strongest contact to the protein shows the most intense NMR signals, enabling mapping of the ligand's binding epitope.[27] The experiments were conducted at the

Table 5. Relative STD Intensities at 900 MHz for Octa-5 and Octa-6 Bound to AT[a]

	H1 ΔU_S	H4 ΔU_S	H1 A′	H4 I	H1 I	H1 A_{NA}	H1 A*	H1 I_S	H4 I_S	*H1* 1,6-anM/G	H3 1,6-anM/G	H2 1,6-anM/G	$COCH_3$
Octa-5	61	35	78	70	74	**89**	**100**(*0.25*)	60	66	*39*	48	30	30
Octa-6	55	28	67	59	68	**76**	**100**(*0.23*)	47	nd	*26*	36	nd	28

[a] The STD NMR values are normalized using the H1 of *N*-sulfo-3,6-disulfated glucosamine (A*) as a reference (100%). The corresponding fractional STD effect values of A* are shown in parentheses.[27]

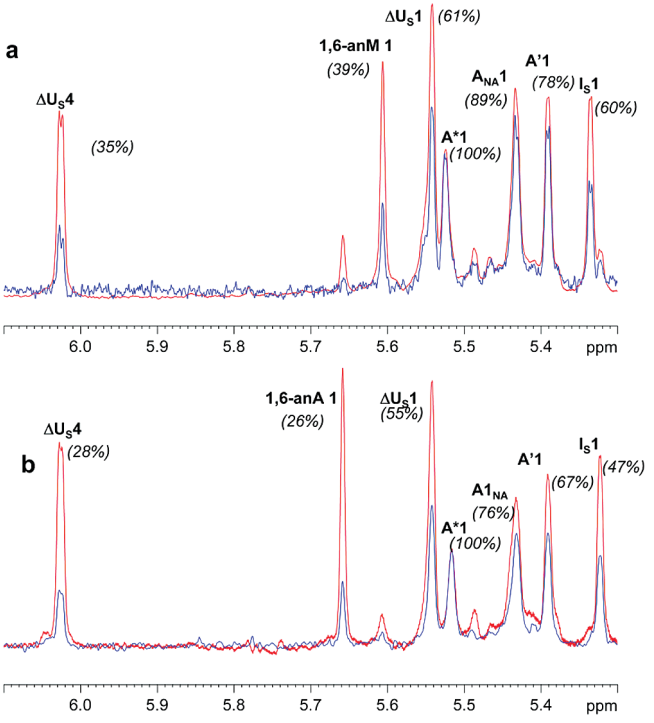

Figure 3. Anomeric region of 900 MHz STD spectra of Octa-5/AT (a) and Octa-6/AT (b) complexes measured at 40:1 molar ratio and 30 °C. Reference and STD spectra are shown in red and blue, respectively.

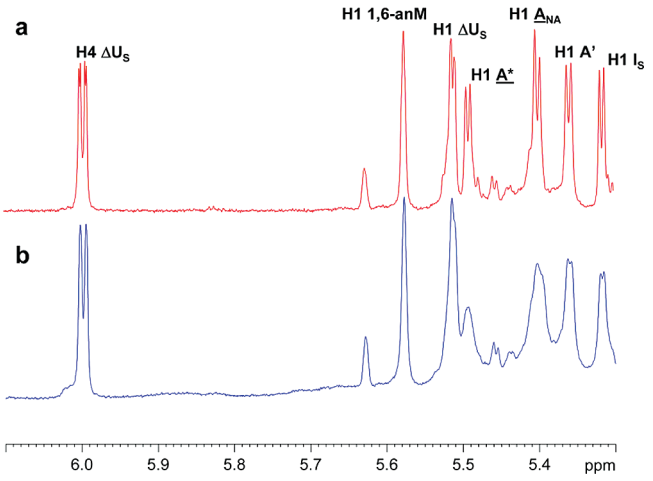

Figure 4. Anomeric region of the 600 MHz proton spectra of Octa-5 in buffer solution (a) and in the presence of AT (b) (ligand:AT molar ratio 10:1).

proton frequency of 900 MHz to minimize signals overlapping and at lower sodium chloride concentration (0.15 M instead at 0.5 M) with respect to octasaccharides previously studied.[19] The difference in the conditions setup is due to the lower AT affinity of these octasaccharides. STD spectra of Octa-5/AT and Octa-6/AT complexes in comparison with their corresponding reference spectra are shown in Figure 3. STD intensities are referred to the most intense STD signal of the spectrum (anomeric protons of A*), and the results are summarized in Table 5. For both octasaccharides, the largest STD effects were observed for the anomeric signal of A* and of the A_{NA} residues within the pentasaccharide sequence (highlighted in bold in Table 5). Weak STD signals were observed for nonreducing ΔU_S residues of all octasaccharides, indicating that this residue is not located in the proximity of the binding region, whereas medium intensity STD signals were observed for the anomeric signal of A′ and both H4 and H1 of I, also belonging to the nonreducing extension of the molecule. In contrast of what was observed for previously studied octasaccharides,[19] weak STD signals were observed among residues of the AGA*IA moiety in both Octa-5 and Octa-6. In fact, whereas the reducing $-I_S$-A disaccharide unit of AGA*IA sequence, similarly to the other pentasaccharide moieties, gave strong STD signals in all previously studied octasaccharides (i.e., Octa-3 and Octa-4),[19] the I_S-1,6-anM and I_S-1,6-anG disaccharides of Octa-5 and Octa-6 show weak STD signals (Table 5). Such an observation is compatible with a minor involvement of this part of the pentasaccharide sequence to the binding with AT. In addition, both octasaccharides showed a small STD effect for the *N*-acetyl signal at 2.08 ppm, indicating that this group is oriented toward the opposite side of the AT surface, as observed in all previously studied octasaccharides.[19] No particular differences between STD profiles of Octa-5 and Octa-6 were observed. The overall reduction of the STD intensities (about 15−20%) observed for Octa-6 with respect to Octa-5 is due to a slightly different protein−ligand ratio of the two octasaccharide/AT complexes.

Conformations of Octasaccharide−AT Complexes. The increase of the line width of proton signals observed in the presence of AT, together with a very small variation of chemical shifts, is consistent with an equilibrium regulated by the intermediate dynamic exchange between the free and bound state. The proton NMR spectra of the Octa-5/AT and Octa-6/AT complexes (10:1 molar ratio), in comparison with the corresponding reference spectra, are shown in Figures 4 and 5, respectively. In the presence of AT, anomeric signal linewidths (H1) of A_{NA} and A* increased considerably in both octasaccharides from 5 to 7 Hz to 15−18 Hz (A_{NA}) and 17−22 Hz (A*), respectively, indicating a strong involvement of the corresponding residues in the binding. On the contrary, a smaller increase of linewidths of H4 of unsaturated uronate and H1 of 1,6-anAS residues (from about 3−4 Hz to 5−6 Hz) was observed for both octasaccharides, in agreement with the higher degree of freedom of these residues and their minor involvement in AT binding. Because cross-relaxation rates differ considerably between the free and bound state, there is a great variation in the cross-peak intensities among two-dimensional NOESY (free state) and transferred-NOESY (bound state) (Tables 6−7).

The role of the conformational equilibrium of iduronate residues in the binding was also investigated by analyzing intraresidue tr-NOE effects. NMR is particularly sensitive to

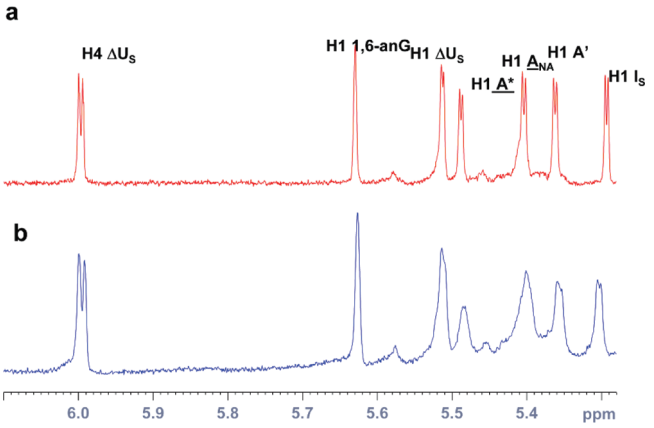

Figure 5. Anomeric region of the 600 MHz proton spectra of Octa-6 in buffer solution (a) and in the presence of AT (b) (ligand:AT molar ratio 10:1).

the presence and relative proportion of conformers. In fact, an H2−H5 NOE was exclusively found in the $^2S_0$ conformer and not observed in the $^1C_4$ form.[15,26] Similarly to what was observed for the previously studied octasaccharides, the H5−H2/H5-H4 NOE ratio of the 2-*O*-sulfated iduronate residue within the AGA*IA sequence of both Octa-5 and Octa-6 significantly increases in the presence of AT (from 0.3 to 1), indicating that the conformation of this residue is driven toward the pure $^2S_0$ form by the protein binding. On the contrary, a smaller enhancement of H5−H2/H5-H4 NOE ratio (from 0.33 to 0.61) was observed for the I residue, suggesting that in this case AT does not induce a complete $^2S_0$ conformer selection. This result partially contrasts to what observed previously for Octa-3,[14] in which the conformation of the corresponding I residue, present almost exclusively in the $^1C_4$ form in free solution, was completely reversed to $^2S_0$ form in the presence of AT. The observed difference with unmodified octasaccharides could be attributed to the steric hindrance generated by the 1,6 anhydro bicyclic ring which disfavor the $^2S_0$ form. A qualitative analysis of the inter-residue tr-NOEs, in comparison with NOEs measured in the absence of AT, indicates that no substantial difference in the glycosidic geometries occurred during the binding (Tables 6−7).

Molecular dynamics and docking procedures (see Experimental Section) are used to build models of Octa-5/AT and Octa-6/AT complexes. Docking procedure was repeated also on Octa-3 under the same conditions. Docked structures of octasaccharide−AT complexes having $A_{NA}GA^*I_SA$ at the same position as that observed in crystal structure, together with clusters having shifted structures along the D-helix of AT, were obtained. To estimate the ability of these models to reproduce the average geometries of the octasaccharide−AT complexes indicated by available NMR data, the magnitudes of theoretical tr-NOEs were calculated using the CORCEMA program.[27] The agreement between the theoretical and experimental tr-NOEs was estimated by calculating *R* factors (see Experimental Section). More specifically, to evaluate the ability of our models to identify the position of octasaccharide residues along the protein binding region regardless their internal conformation, trNOEs of H1−H2 protons cross-relaxing within aminosugar residues were analyzed. Complexes having $A_{NA}GA^*I_SA$ at the same position observed in the structure of pentasaccharide−AT cocrystals,[29] showed a good fitting between theoretical and experimental data, whereas those having shifted structures along the D-helix of AT gave

Table 6. Experimental Intra- and Inter-residues NOESY (in Parentheses) and tr-NOESY Values of OCTA-5 in Buffer Solution and in the Complex with AT at Three Different Mixing Times

		100 ms	200 ms	300 ms
		Intraresidue		
H1 ΔU_S	H2	4.7	9.3	18.3 (1.6)
H1 A′	H2	15.2	25.5	37.9 (9.0)
H5 I	H4	15.1	25.2	37.7 (5.9)
	H2	7.0	14.7	23.1 (2.0)
H1 A_{NA}	H2	9.6	16.4	15.6 (7.8)
H1 A*	H2	17.7	28.5	44.4 (6.1)
H5 I_S	H4	14.0	26.9	37.5 (5.0)
	H2	11.7	23.0	39.2 (1.6)
H1 1,6-anM	H2	11.8	19.3	30.2 (3.0)
		Inter-residue		
H1 ΔU_S	H6 A′	3.0	7.3	12.6 (2.2)
	H6′ A′	1.7	4.9	7.8 (0)
	H4 A′	9.2	15.4	24.6 (3.5)
H1 A′	H3 I	16.5	27.3	37.7 (9.4)
	H4 I	9.9	16.3	24.8 (5.2)
H1 I	H4 A_{NA}	16.8	28.7	38.9 (3.4)
H1 A_{NA}	H4 G	17.3	29.7	42.0 (4.5)
H1 A*	H3 I_S	8.7	14.8	23.5 (6.1)
	H4 I_S	5.9	9.2	17.6 (4.4)
H1 I_{2S}	H5 1,6-anM	5.2	10.3	21.8 (2.1)
	H4 1,6-anM	14.0	23.2	39.0 (2.6)

Table 7. Experimental Intra- and Inter-residues NOESY (in Parentheses) and tr-NOESY Values of OCTA-6 in Buffer Solution and in the Complex with AT, at Three Different Mixing Times

		100 ms	200 ms	300 ms
		Intraresidue		
H1 ΔU_S	H2	6.4	10.9 (nd)	22.1
H1 A′	H2	10.7	19.9 (5.4)	32.5
H5 I	H4	11.3	21.5 (4.0)	27.7
	H2	5.9	11.1 (1.2)	17.5
H1 A_{NA}	H2	9.2	13.6 (4.5)	21.6
H1 A*	H2	7.8	12.2 (4.9)	16.5
H5 I_S	H4	9.7	20.8 (3.4)	30.2
	H2	8.9	18.9 (1.1)	32.5
H1 1,6-anG	H2	4.0	7.3 (0.8)	12.5
		Inter-residue		
H1 ΔU_S	H6 A′	4.4	6.4 (1.2)	11.9
	H6′ A′	2.5	3.7 (nd)	7.4
	H4 A′	8.1	13.8 (1.8)	22.6
H1 A′	H3 I	14.0	24.0 (6.6)	33.7
	H4 I	8.0	14.4 (3.4)	19.8
H1 I	H4 A_{NA}	14.7	27.3 (6.3)	41.3
H1 A_{NA}	H4 G	12.3	21.8 (2.8)	34.5
H1 A*	H3 I_S	12.2	28.6 (3.5)	38.2
	H4 I_S	9.5	19.4 (2.6)	30.1
H1 I_{2S}	H5 1,6-anG	6.4	11.0 (1.6)	18.8
	H4 1,6-anG	9.9	16.5 (1.5)	29.2

significantly higher *R* factors. Moreover, in disagreement with STD results, these shifted models present also the octasaccharide rotated along a direction parallel to the D-helix, with the *N*-acetyl group oriented toward the opposite side of the AT surface. (Table 8) (Supporting Information Figure S10). Docking output models of Octa-5, Octa-6, and Octa-3 that satisfy tr-NOESY data take similar positions in the AT binding site (Figures 6−7). In these assemblies, distances between the pentasaccharide moiety and AT are on the average shorter than those between the nonreducing ΔU_S-A′-I− moiety and the protein binding region (Figure 8).

Table 8. *R* Factor Average Values Calculated by Fitting between Experimental and Theoretical tr-NOEs of H1−H2 protons Cross-Relaxing within Hexosamine Residues[a]

	A′	A_{NA}	A*	1,6-anM/G
Octa-3	**0.21** (**0**)	**0.18** (**3**)	**0.05** (**3**)	**0.13** (**5**)
Octa-5	**0.29** (**0**)	**0.27** (**2**)	**0.21** (**4**)	**0.08** (**1**)
Octa-5 shifted	**0.28**	0.40	**0.15**	**0.07**
Octa-5 inverted	0.40	0.39	0.50	0.31
Octa-6	**0.22** (**1**)	**0.13** (**1**)	**0.31** (**2**)	**0.04** (**1**)

[a] Values were averaged for different octasaccharide−AT complexes obtained from docking and cluster analysis. Each complex is represented by an ensemble of three or four geometries with an rmsd distance less than 2 Å. In brackets, the error at the last decimal digit is given by a standard deviation measurement. *R* Factors calculated on a shifted (Octa-5 shifted) and an inverted (Octa-5 inverted) octasaccharide−AT complexes were also reported. Thin fonts indicate poor fitting with the experimental data.

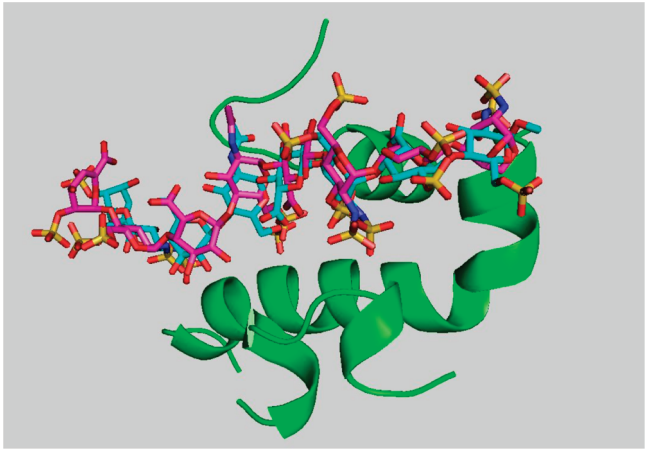

Figure 6. Superimposition of Octa-5/AT (magenta) and Octa-3/AT (cyan) model complexes obtained by rigid docking simulation. The AT binding region is shown in green.

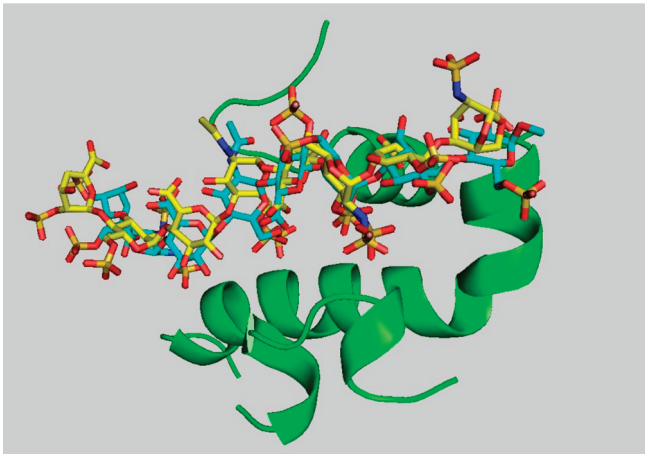

Figure 7. Superimposition of Octa-6/AT (yellow) and Octa-3/AT (cyan) model complexes obtained by rigid docking simulation. The AT binding region is shown in green.

However, whereas distances between the majority of sugar residues of Octa-5 and Octa-6 and the AT interacting amino acids are similar to those measured for Octa-3, the terminal 1,6-anG/M residues are more distant from Arg46 and Arg47 than the terminal *N*-sulfo-glucosamine-6-*O*-sulfate residue of Octa-3. Moreover, the average distance between the *N*-sulfo group of 1,6-anhydro residues and AT is significantly larger for 1,6-anG than that of 1,6-anM (about 0.75 nm

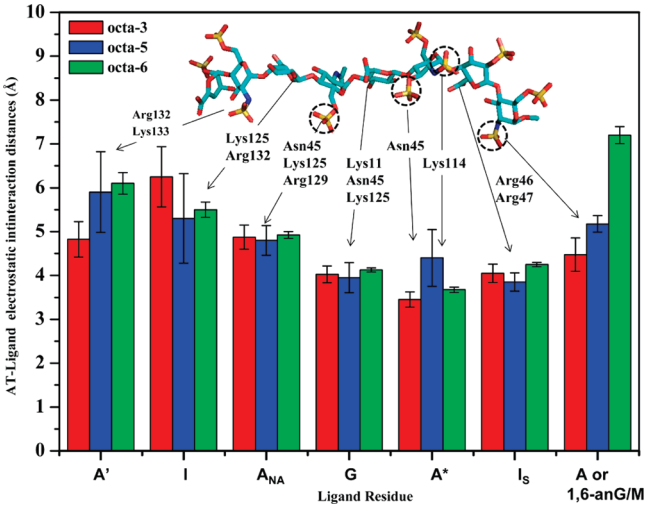

Figure 8. Schematic representation of the individual side chain interactions showing average contact distances between octasaccharide residues and AT (Octa-3, Octa-5, and Octa-6 red, blue, and green bars, respectively). Each distance is averaged on two or three ligand−AT contacts on the ensemble of four docking ligand−AT complex generated structures, selected from those that better agree with experimental data (trNOESY). Distance standard deviation is shown on the top of each column. Distances are taken between the heteroatom of the monosaccharide interacting group (−**S**O_3, −**C**OO, or **C**H-OH) and those of nearest AT aminoacids. Octa-3 structure is shown at the top of the figure, with sulfated groups in the AGA*IA sequence essential for AT binding highlighted by dashed circles.

versus 0.5 nm), in agreement with the lower affinity observed for Octa-6 (Figure 8, Table 1). On the contrary, the terminal unmodified residue of Octa-3 shows an average distance from AT comparable to that of the other A_{NA}GA*I_SA residues, indicating its stronger involvement in the binding. These results are in a good agreement with the observed STD effects experimentally determined on proton signals of the same residues (Table 5).

Discussion and Conclusions

Understanding of the mechanism of interaction between proteins and oligosaccharides of heparin and of its analogue heparan sulfate is a major challenge in GAG research.[30] Sequence specificity for protein binding and activity has emerged, showing that it is the combination of overall conformation, charge distribution, and flexibility exhibited by heparin/heparan sulfate saccharides that determines the extent of protein binding and related activity.[31] However, the lack of well-defined model compounds containing a sufficient structural diversity in terms of sulfation pattern and sequences, often prevented in depth studies. Although correlations between structure, affinity for AT and anti-FXa activity have been obtained for A_{NA}GA*I_SA-related heparin synthetic oligosaccharides as large as hexasaccharide,[10] similar information is missing for longer oligosaccharides terminating with unusual residues. A small effect of 1,6-anhydro residues at the reducing end as observed for experimental enoxaparin-like LMWHs[32] is conceivably attributable only to chains also containing the A_{NA}GA*I_SA sequence or a modified form of it.

In the present work, two novel AT-binding octasaccharides containing an 1,6-anM and 1,6-anG residue, respectively, at the reducing end (Octa-5 and Octa-6) have been isolated from

enoxaparin. Even if the presence of terminal 1,6-anhydro rings have been previously described as a major structural fingerprint of enoxaparin,[17,18] the present octasaccharides have the peculiarity to bear an 1,6-anM or 1,6-anG instead of the terminal *N*-sulfo,6-*O*-sulfo-glucosamine of the active pentasaccharide $A_{NA}GA^*I_SA$. The AT binding properties of both Octa-5 and Octa-6 were measured and compared with those previously described for Octa-3 that contains the unmodified pentasaccharide at the reducing end.

Fluorescence titrations indicated that the affinity for AT of these octasaccharides is characterized by equilibrium dissociation constants about 10- and 50-fold lower than those measured for Octa-3 and the synthetic pentasaccharide fondaparinux, respectively. Such evidence confirms that the lack of 6-*O* sulfo group of the terminal glucosamine residue A_{NA} of the pentasaccharide sequence $A_{NA}GA^*I_SA$, together with the unusual conformation of the residue bearing the 1,6-anhydro cycle, results in weaker binding to AT. However, the decreasing in affinity for AT of Octa-5 and Octa-6 with respect to fondaparinux was much larger than that observed just by the removal of 6-*O*-sulfo group of the terminal reducing glucosamine of the pentasaccharide.[13] Although affinity values obtained from the present and previous studies are not directly comparable due to somewhat different experimental conditions, the relatively larger difference found suggested also that the bicyclic structure of the 1,6-anhydro residues might sterically interfere on the interaction with AT. Reduction in AT-binding affinity is correlated with a lower anti-FXa activity of Octa-5 and Octa-6 compared to both fondaparinux and enoxaparin (Table 2). Importantly, enoxaparin shows a slight decrease in anti-FXa-activity (13%) in human plasma compared to measurement in aqueous buffer solution, which could be due to unspecific protein binding (i.e., albumin) of some AT binding components. In contrast, the activities of Octa-5 and Octa-6 are almost the same in plasma and in aqueous solution, suggesting a specific interaction of both compounds with AT (Table 2). This was also confirmed from STD and docking results, showing that the closest contacts with AT involve the residues of the octasaccharide belonging to the sequence $A_{NA}GA^*I_SA$ and correspond to the A_{NA}-GA*− moiety for both Octa-5 and Octa-6. On the contrary of what was observed for Octa-3,[19] weaker STD signals for the terminal $-I_S$-1,6-anM/G disaccharides with respect to those of the −AGA*− moiety were observed, indicating a larger distance of these residues from AT. Moreover, only model outputs having the $A_{NA}GA^*I_SA$ sequence in the same position adopted in the pentasaccharide−AT complex can interpret both STD and tr-NOE data. Although our models are not sufficiently accurate to define the complex at atomic level precision due to the lack of suitable molecular dynamic force field description able to satisfy conformational behavior of highly charged molecules,[33] they clearly show that the $-A_{NA}$-G-A*-I_S sequence of the pentasaccharide moiety is in closer contact with AT than the trisaccharide moiety ΔU_S-A′-I− at the nonreducing end and the terminal 1,6an-AS residues at the reducing end (Figure 8).

Besides the larger average distances between AT amino acids and terminal 1,6-anM/G residue measured for both Octa-5 and Octa-6 with respect to Octa-3, significant differences were found between the two isomers. Octa-6 shows higher averaged distance between the *N*-SO_3 group of its terminal residue and both Arg46 and Arg47 with respect to Octa-5 (Figure 8), paralleling the lower affinity to AT measured for this octasaccharide. The single interaction of the *N*-SO_3 group in terminal 1,6-anhydro residues is expected to reduce the strength of ionic interactions between the reducing part of the pentasaccharide and AT with respect to unmodified *N*,6-*O*-sulfated glucosamine. However, even if the absence of the 6-*O*-sulfo group in the terminal A residue reduces the affinity to AT,[13] no ionic interactions have been observed between this group and the positively charged amino acid of AT.[10,13] The observed higher affinity of $A_{NA}GA^*I_SA$ containing oligosaccharides, due also to the contribution of the 6-*O*-sulfo group on the terminal A residue, can be explained by the increasing of population of the skew $^2S_0$ conformer of the neighbor I_S residue,[15] as indicated by different $^3J_{H-H}$ values of I_S measured on Octa-3 with respect to those of Octa-5 and Octa-6.[14] In fact, the higher affinity to AT of an heparin pentasaccharide, bearing an extra sulfate group at C-3 of the terminal A residue, was proposed to be the consequence of a high population (about 90%) of the $^2S_0$ conformer.[34] Moreover, the present results suggest that the *manno* configuration of the 1,6-anhydro residues promotes a better interaction with AT with respect to the *gluco* form due to its favorite position of the *N*-SO_3 group (Figure 8). Despite their modest anti FXa activity, those 1,6 anhydro modified oligosaccharides display a specific antithrombotic activity which cannot be neglected in the overall biological profile of the LMWH complex mixture. From a practical point of view, because the depolymerization condition used to prepare enoxaparin strongly affect the content of 1,6-anhydro residues, as well as the relative contents of their *manno* and *gluco* epimers, control of the overall composition and activity requires an accurate optimization of the manufacturing procedures.

A more detailed understanding of the role of structural variations on AT binding properties of heparin oligosaccharides may help in the synthesis of ligand analogues and in the design of new LMWHs with an appropriate structure to ensure high affinity to AT. However, structural refinement of the obtained structures by means of methods such as full molecular dynamics simulations or ab initio calculations is also necessary to fully interpret experimental data.

Experimental Section

Octasaccharide Isolation and Purification. General procedure for the isolation, purification, and sequencing of Octa-5 and -6 (Figure 1) was obtained by combining AT affinity chromatography and cetyltrimethylammonium-strong anion-exchange (CTA-SAX) chromatography on a semipreparative scale, starting from gel permeation chromatographic (GPC) octasaccharide fractions of enoxaparin and following the experimental conditions previously described.[19]

Fluorescence Titration. The equilibrium constant K_d for the interaction of AT with the various oligosaccharides was monitored at 25 °C in 0.05 M HEPES pH 7.4 containing 0.1 M NaCl by following the enhancement of the serpin intrinsic fluorescence (λ_{ex} = 280 nm, λ_{em} = 340 nm) upon its reaction with increasing concentrations of the products, a usual procedure.[19] A RF5000 Shimadzu fluorospectrophotometer equipped with a thermostatted cell holder was used to perform the fluorescence intensity measurements. K_d was also determined in the presence of 0.25 M NaCl (Octa-5, Octa-6, and fondaparinux) and 0.5 M NaCl (Octa-3 and fondaparinux). The best estimate of K_d, the equilibrium dissociation constant for the studied interactions, was obtained from the fluorescence data by nonlinear regression analysis as previously described.[19]

Measurement of Antifactor Xa Activity. Anti-Xa activity was determined with ACL 7000 automated coagulation instrument (Instrumentation Laboratory) using Heparin-kit (Instrumentation Laboratory) containing AT, FXa, and the chromogenic substrate

S-2765. The assay was exactly performed according to the manufacturer's instructions. The second international standard for LMWH (National Institute for Biological Standards and Control, London, UK, established in 2003, code no. 01/608) was used to construct a standard calibration curve. On the basis of a common calibration curve elaborated with the second international LMWH -standard, we assayed anti-FXa-activity of Octa-5 and Octa-6 and compared them with our two reference compounds, enoxaparin and fondaparinux. Enoxaparin, Octa-5, and Octa-6 were tested at the concentration of 10 μg/mL, whereas fondaparinux was tested at 1 μg/mL. Briefly, test agents or the international LMWH standards were first diluted in human standard plasma (Instrumentation Laboratory) or buffer (0.05 M Tris HCl, 0.154 M NaCl, pH 7.4). Test agents containing samples in plasma or buffer were further diluted 1:20 with a buffer containing AT and placed in duplicates into the probing rotor. Factor Xa reagent and chromogenic substrate were filled into designated reservoirs of the ACL 7000 automated coagulation instrument. The anti-Xa activity assay was run with the protocol "Heparin" integrated in the ACL 7000 software. During the assay, 50 μL of the sample diluted with buffer were mixed with 50 μL of factor Xa reagent. After incubation time for 60 s at 37 °C, 50 μL of 1.1 mM chromogenic substrate was added and the changes in absorbance as a function of time were measured at wavelength of 405 nM. The specific anti-FXa activity for test agents was calculated by using the exponential curve fit function of Microsoft Excel 2003. The calibration curve was constructed with the second international standard for LMWH (code no. 01/608).

NMR Spectra. All monodimensional and bidimensional NMR spectra were measured at 30 °C, at 600 and 900 MHz, both with a Bruker Avance spectrometers equipped with a high-sensitivity 5 mm TCI cryoprobe. For proton detection, 350 μg of octasaccharide samples was dissolved in ^2H_2O (99.9%) and freeze-dried to remove residual water. After exchanging the samples three times, samples were dissolved in 0.7 mL of 10 mM phosphate buffer (0.15 M NaCl, pH 7.4) with 3 mM EDTA in ^2H_2O (99.996%). For the binding studies, samples were prepared by dissolving 200 μg and 400 μg of each octasaccharide in the phosphate buffer so as to reach a 1:10 or 1:40 AT/octasaccharide molar ratio for tr-NOESY and STD experiments, respectively. Proton spectra were recorded with presaturation of the residual water signal, with a recycle delay of 8 and 128 scans. Double-quantum-filter correlation spectroscopy (DQFCOSY) and TOCSY spectra were acquired using 32 scans per series of 2K × 512W data points with zero filling in F1, and a shifted squared cosine function was applied prior to Fourier transformation. All NOESY (nuclear Overhauser enhancement spectroscopy) and transferred NOESY experiments were performed with a total of 48 scans collected for each free-induction decay (matrix 2048 × 512 points) and data were zero-filled to 4K × 2K points before Fourier transformation. Mixing time values of 100, 200, and 300 ms were used. The pulse sequence used for the monodimensional STD experiments includes a 25 ms spin-lock pulse to eliminate the broad resonances of the protein and water suppression. A train of 40 Gaussian-shaped pulses of 50 ms each was applied to produce selective saturation. The on-resonance irradiation was performed at the low field protein resonances (7.25 ppm), whereas the off-resonance control irradiation was performed at 24 ppm. The number of scans and dummy scans were 1024 and 16, respectively.

Computational Studies on Octasaccharide−AT Complexes. The octasaccharide models were created by Macromodel version 4.0 starting from previously reported structures,[19,35] where I and I_S were in $^2S_0$ conformation while glucosamines and glucuronic acid residues were in $^4C_1$ conformation, as shown from NMR experimental evidence. Molecular dynamics (MD) simulation of Octa-3, Octa-5, and Octa-6 was performed using AMBER* force field included in the MAESTRO 8.0/Macromodel simulation package, and the Macromodel batchmin simulation engine was used for MD trajectory production. Simulations were done on models where each octasaccharide molecule was enveloped by a water molecules layer at least 12 Å wide. To do that, the free code software "solvate-1.0" (Helmut Grubmüller and Volker Groll Theoretical and Computational Biophysic Group, Max Planck Institute) was used. After a short simulation time dynamics (about 400 ps), Octa-3, Octa-5, and Octa-6 models were checked in each residue conformation to agree qualitatively with the experimental seen. Glycosidic geometries of the I_S-1,6-anG/M disaccharides were set according to H1−H4 and H1−H5 inter-residue distances on the basis of values extrapolated from experimental NOE magnitudes. Octa-3, Octa-5, and Octa-6 geometries so obtained were used as ligands for automatic docking octasaccharide−AT complex structure determination. Docking simulation was performed using Autodock 4.2 program. The receptor (AT) geometry was taken from PDB file (Protein Data Bank 1AZX[29]). Explicit treatment of every hydrogen was used for both ligand and receptor, while atom charges were calculated following the Gasteiger approach.[36] Ligands were treated as a rigid object, fixing all glycosidic torsional degrees of freedom, while hexocyclic functional group torsional angles (32 degrees of freedom for each complex) were allowed to move during docking simulation. About 100 complex geometries were generated using a Lamarckian Genetic Algorithm with local search, characterized by the following set of parameters: population size was fixed to 500, maximum number of energy evaluation per run was chosen to be 5×10^6, and 2.7×10^5 maximum generation number. Others parameters were left as default settings. Results were analyzed by a fast cluster analysis: generated complex geometries were ranked by a rmsd cutoff of 2.0 Å. After ranking, a few clusters with higher score function and/or most populated having the $A_{NA}GA^*I_SA$ sequence in the same position as found in the crystal structure of the pentasaccharide−AT complex[29] were considered to fit tr-NOESY data. Less populated clusters, having the octasaccharides moved up toward the nonreducing end by about a disaccharide unit from the normal AT binding site, were also found and considered. To evaluate the ability of all these complex models to interpret the position of the ligand in the AT binding site, the magnitudes of theoretical tr-NOEs were calculated on different models of octasaccharide−AT complexes using the CORCEMA program.[28] The agreement between the theoretical and experimental tr-NOEs was evaluated by calculating the fitting quality parameter R factors as defined in eq 1.

$$R^2 = \frac{\sum_{t_{mix}} (\mathrm{NOE}^{exp}(t_{mix}) - \mathrm{NOE}^{CALC}(t_{mix}))^2}{\sum_{t_{mix}} (\mathrm{NOE}^{exp}(t_{mix}))^2} \quad (1)$$

R Factor values higher than 0.3 are indicative for a pour local structure description. The values of the dissociation constant (K_d) used to calculate theoretical trNOEs were based on those calculated by equilibrium titration and published data.[19] The correlation times of AT and octasaccharides were considered as isotropic and estimated from the previous data.[11,19,37] However, due to the slightly different condition used (temperature and ion strength), the K_d and the off-rate (k_{off}) used in the calculations varied during the optimization (K_d and k_{off}: 0.1 mM and 50 s^{-1}, respectively).

Acknowledgment. The 900 MHz spectra were recorded at the SON NMR Large Scale Facility in Utrecht, by the financial support of the Access to Research Infrastructures activity in the sixth Framework Programme of the EC (contract no. RII3-026145, EU-NMR).

Supporting Information Available: NMR spectra of octasaccharides 5 and 6 and of disaccharide and tetrasaccharide models (HSQC, NOESY, and ROESY), model of Octa-5/AT complex

shifted along the AT binding site, chemical shift tables of disaccharide and tetrasaccharide models. This material is available free of charge via the Internet at http://pubs.acs.org.

References

(1) Gray, E.; Mulloy, B.; Barrowcliffe, T. W. Heparin and low-molecular-weight heparin. *Thromb. Haemostasis* **2008**, *99*, 807–818.
(2) Linhardt, R. J. Heparin: Structure and Activity. *J. Med. Chem.* **2003**, *46*, 2551–2554.
(3) Mousa, S. A. Heparin and low molecular weight heparin in thrombosis and inflammation: emerging link. In *Chemistry and Biology of Heparin and Heparan Sulfate*; Garg, H. G., Linhardt, R. J., Hales, C. A., Eds; Elsevier Ltd.: New York, 2005; pp 571−581.
(4) Casu, B.; Lindahl, U. Structure and biological interactions of heparin and heparan sulfate. *Adv. Carbohydr. Chem. Biochem.* **2001**, *57*, 159–206.
(5) Loganathan, D.; Wang, H. M.; Mallis, L. M.; Linhardt, R. J. Structural variation in the antithrombin III binding site region and its occurrence in heparin from different sources. *Biochemistry* **1990**, *29*, 4362–4368.
(6) Viskov, C.; Just, M.; Laux, V.; Mourier, P.; Lorenz, M. Description of the chemical and pharmacological characteristics of a new hemisynthetic ultra-low-molecular-weight heparin, AVE5026. *J. Thromb. Haemostasis* **2009**, *7*, 1143–1151.
(7) Bisio, A.; Vecchietti, D.; Citterio, L.; Guerrini, M.; Raman, R.; Bertini, S.; Eisele, G.; Naggi, A.; Sasisekharan, R.; Torri, G. Structural features of low-molecular-weight heparins affecting their affinity to antithrombin. *Thromb. Haemostasis* **2009**, *102*, 865–873.
(8) Zang, Z.; Weiwer, M.; Li, B.; Kemp, M. M.; Daman, T. H.; Linhardt, R. J. Oversulfated chondroitin sulfate: impact of heparin impurity, associated with adverse events, on low-molecular-weight heparin preparation. *J. Med. Chem.* **2008**, *51*, 5498–5501.
(9) Lane, D. A.; Denton, J.; Flynn, A. M.; Thunberg, L.; Lindahl, U. Anticoagulant activities of heparin oligosaccharides and their neutralization by platelet factor 4. *Biochem. J.* **1984**, *218*, 725–732.
(10) Petitou, M.; van Boeckel, C. A. A synthetic antithrombin III binding pentasaccharide is now a drug! What comes next? *Angew. Chem., Int. Ed.* **2004**, *43*, 3118–3133.
(11) Hricovini, M.; Guerrini, M.; Bisio, A.; Torri, G.; Petitou, M.; Casu, B. Conformation of heparin pentasaccharide bound to antithrombin III. *Biochem. J.* **2001**, *359*, 265–272.
(12) Chen, J.; Jones, C. L.; Liu, J. Using an enzymatic combinatorial approach to identify anticoagulant heparan sulfate structures. *Chem. Biol.* **2007**, *14*, 986–993.
(13) van Boeckel, C. A. A.; Petitou, M. The unique antithrombin III binding domain of heparin: a lead to new synthetic antithrombotics. *Angew. Chem., Int. Ed.* **1993**, *32*, 1671–1818.
(14) Guerrini, M.; Guglieri, S.; Beccati, D.; Torri, G.; Viskov, C.; Mourier, P. Conformational transitions induced in heparin octasaccharides by binding with antithrombin III. *Biochem. J.* **2006**, *399*, 191–198.
(15) Ferro, D. R.; Provasoli, A.; Ragazzi, M.; Casu, B.; Torri, G.; Bossennec, V.; Perly, B.; Sinay, P.; Petitou, M.; Choay, J. Conformer populations of L-iduronic acid residues in glycosaminoglycan sequences. *Carbohydr. Res.* **1990**, *195*, 157–167.
(16) Linhardt, R. J.; Gunay, N. S. Production and chemical processing of low molecular weight heparins. *Semin. Thromb. Hemostasis* **1999**, *25* (Suppl 3), 5–16.
(17) Guerrini, M.; Guglieri, S.; Naggi, A.; Sasisekharan, R.; Torri, G. Low molecular weight heparins: structural differentiation by bidimensional nuclear magnetic resonance spectroscopy. *Semin. Thromb. Hemostasis* **2007**, *33*, 478–487.
(18) Mourier, P.; Viskov, C. US Patent 2005/0119477 A1, 2005; *Chem. Abstr.* **2005**, *142*, 89363.
(19) Guerrini, M.; Guglieri, S.; Casu, B.; Torri, G.; Mourier, P.; Boudier, C.; Viskov, C. Antithrombin-binding octasaccharides and role of extensions of the active pentasaccharide sequence in the specificity and strength of interaction. *J. Biol. Chem.* **2008**, *283*, 26662–26675.
(20) Mourier, P. A. J.; Viskov, C. Chromatographic analysis and sequencing approach of heparin oligosaccharides using cetyltrimethylammonium dynamically coated stationary phases. *Anal. Biochem.* **2004**, *332*, 299–313.
(21) Höök, M.; Björk, I.; Hopwood, J.; Lindahl, U. Anticoagulant activity of heparin: separation of high-activity and low-activity heparin species by affinity chromatography on immobilized antithrombin. *FEBS Lett.* **1976**, *66*, 90–93.
(22) Low molecular mass heparin. *European Pharmacopoeia 01/2008:0828*, 6.0 ed.; European Directorate for the Quality of Medicine & HealthCare: Strasbourg, January, 2008.
(23) Herbert, J. M.; Hérault, J. P.; Bernat, A.; Van Amsterdam, R. G. M.; Vogel, G. M. T.; Lormeau, J. C.; Petitou, M.; Meuleman, D. G. Biochemical and pharmacological properties of SANORG3232701. *Circ. Res.* **1996**, *79* (3), 590–600.
(24) Mascellani, G.; Guerrini, M.; Torri, G.; Liverani, L.; Spelta, F.; Bianchini, P. Characterization of di- and monosulfated, unsaturated heparin disaccharides with terminal *N*-sulfated 1,6-anhydro-β-D-glucosamine or *N*-sulfated 1,6-anhydro-β-D-mannosamine residues. *Carbohydr. Res.* **2007**, *342*, 835–842.
(25) Černy, I.; Buděšinsky, M.; Trnka, T.; Cěrny, M. Preparation of 2-amino-1,6-anhydro-2,3-dideoxy-β-L-arabino-hexopyranose. ^{1}H- and ^{13}C-NMR spectra of deoxy derivatives of 2-amino-1,6-anhydro-2-deoxy-D-glucose and 2-amino-1,6-anhydro-2-deoxy-D-mannose. *Carbohydr. Res.* **1984**, *130*, 103–114.
(26) Ferro, D. R.; Provasoli, A.; Ragazzi, M.; Torri, G.; Casu, B.; Gatti, G.; Jacquinet, J. C.; Sinay, P.; Petitou, M.; Choay, J. Evidence for conformational equilibrium of the sulphated L-iduronate residue in heparin and in synthetic heparin mono- and oligosaccharides: NMR and force-field studies. *J. Am. Chem. Soc.* **1986**, *108*, 6773–6778.
(27) Mayer, M.; Meyer, B. Group epitope mapping by saturation transfer difference NMR to identify segments of a ligand in direct contact with a protein receptor. *J. Am. Chem. Soc.* **2001**, *123*, 6108–6117.
(28) Moseley, H. N.; Curto, E. V.; Krishna N. R. Complete relaxation and conformational exchange matrix (CORCEMA) analysis of NOESY spectra of interacting systems; two-dimensional transferred NOESY. *J. Magn. Reson., Ser. B* **1995**, *108*, 243−261.
(29) Jin, L.; Abrahams, J. P.; Skinner, R.; Petitou, M.; Pike, R. N.; Carrell, R. W. The anticoagulant activation of antithrombin by heparin. *Proc. Natl. Acad. Sci. U.S.A.* **1997**, *94*, 14683–14688.
(30) Lindahl, U.; Li, J.P.. Interaction between heparan sulfate and proteins—design and functional implications. *Int. Rev. Cell Biol.* **2009**, *276*, 105–159.
(31) Deakin, J. A.; Blaum, B. S.; Gallagher, J. T.; Uhrín, D.; Lyon, M. The binding properties of minimal oligosaccharides reveal a common heparan sulfate/dermatan sulfate-binding site in hepatocyte growth factor/scatter factor that can accommodate a wide variety of sulfation patterns. *J. Biol. Chem.* **2009**, *284*, 6311–6321.
(32) Jeske W. P.; Neville B.; Ma Q.; Hoppensteadt D. A.; Fareed J. Effect of 1,6-anhydro bicyclic ring structure on the pharmacokinetic and pharmacodynamic behavior of low molecular weight heparin. *Blood* (ASH Annual Meeting Abstracts) **2004**, *104*, abstract 1868.
(33) Forster, M; Mulloy, B. Computational approaches to the identification of heparin-binding sites on the surfaces of proteins. *Biochem. Soc. Trans.* **2006**, *34*, 431–434.
(34) Petitou, M.; Jaurand, G.; Derrien, M.; Duchaussoy, P.; Choay, J. A new, highly potent, heparin-like pentasaccharide fragment containing a glucose residue instead of a glucosamine. *Bioorg. Med. Chem. Lett.* **1991**, *1*, 95–98.
(35) Mulloy, B.; Forster, M. J.; Jones, C.; Davies, D. B. NMR molecular modeling studies of the solution conformation of heparin. *Biochem. J.* **1993**, *293*, 849–858.
(36) Gasteiger, J.; Marsili, M. Iterative partial equalization of orbital electronegativity—a rapid access to atomic charges. *Tetrahedron* **1980**, *30*, 3219–3228.
(37) Angulo, J.; Hricovini, M.; Gairi, M.; Guerrini, M.; de Paz, J. L.; Ojeda, R.; Martín-Lomas, M.; Nieto, P. Dynamic properties of biologically active synthetic heparin-like hexasaccharides. *Glycobiology* **2005**, *15*, 1008–1015.